ABSTRACT

ZHANG, SHENGWEI. Towards Single-molecule Fluorescence Microscopy on a Mobile Phone Using Plasmonic Nanohole. (Under the direction of Dr. Qingshan Wei).

Single-molecule detection plays an increasingly important role in biological science and material science. Traditional microscopy and spectroscopy approach require bulky and expensive instrument, which limits its applications in advanced laboratory settings. Recent years have witnessed the development of cellphone-based optical sensing and imaging system. With these devices, optical imaging and detection of nanoscale or molecular objects in the field settings have been demonstrated including DNA imaging, single nanoparticle imaging, and virus imaging. However, single molecule sensitivity has not been achieved on the mobile phone. With the help of surface plasmon resonance property of nanostructure of noble metals, fluorescence signal can be enhanced. In this work, we attempt to reach ultimate single-molecule sensitivity on a cellphone-based imaging device with nanohole enhanced fluorescence. To reach this goal, nanohole-enhanced fluorescence will be applied to cellphone fluorescence microscopy. Nanohole array used for fluorescence enhancement was fabricated and characterized. For initial testing, benchtop tests were made to quantify fluorescence enhancement performance and optimize parameters of nanohole array. A smartphone reader device was also designed, assembled and characterized as a part of collaboration project, which is also planned to be used on the imaging of single molecule as a portable mobile platform.

Towards Single-molecule Fluorescence Microscopy on a Mobile Phone Using Plasmonic Nanohole.

by
Shengwei Zhang

A thesis submitted to the Graduate Faculty of
North Carolina State University
in partial fulfillment of the
requirements for the degree of
Master of Science

Chemical Engineering

Raleigh, North Carolina
2019

APPROVED BY:

Qingshan Wei
Committee Chair

Orlin D. Velev

Michael D. Dickey

BIOGRAPHY

Shengwei Zhang was born in Tianjin, China. He studied macromolecular materials and engineering at Zhejiang University in China from 2012 to 2016 and graduated with B. E. degree. During his undergraduate study, he participated in the Student Research Training Program (SRTP) and National Undergraduate Training Programs for Innovation and Entrepreneurship. In his undergraduate research, he focused on synthesis and characterization of polymeric micelle based nano drug delivery system. During the summer of his junior year, he worked as a summer intern in Dr. Marjorie Longo's lab at chemical engineering department, UC Davis. During his stay, he was involved with the study of surfactant adsorption on graphite surface using atomic force microscopy (AFM). In September 2017, he started graduate studies in the department of chemical and biomolecular engineering at North Carolina State University. In January 2018, he joined Dr. Qingshan Wei's research group as graduate research assistant. His research focuses are single-molecule imaging and designing mobile phone imaging platform.

ACKNOWLEDGMENTS

I would like to express my sincere gratitude to my advisor, Dr. Qingshan Wei for his guidance and support in my research projects. His suggestions are valuable in helping me reaching the goal. This thesis would not be possible without his lasting support and advice. I also appreciate the help and comments from my committee members, Dr. Velev and Dr. Dickey. Their constructive advice and suggestions are very helpful in my research.

I would also like to thank everyone at Wei group who have helped me during my research. I would like to acknowledge the staff at the Analytical Instrument Facility (AIF) and Nanofabrication Facility (NNF) for their help and training on the instrument. Last, I would like to thank all of my friends and my family members, for their constant support and encouragement.

TABLE OF CONTENTS

LIST OF FIGURES

CHAPTER 1: Introduction

1.1 Single-molecule detection

The origin of single-molecule microscopy dates back to the pioneering work from Moerner and Kador, who used absorption to detect dye molecules embedded in a crystalline matrix at cryogenic temperatures. [1] In the past twenty years, single-molecule microscopy reached increasing importance in biological reaction kinetics and enzymatic reaction. A number of single-molecule detection techniques have been applied in protein and nucleic acid detection in low concentrations, protein dynamics study and DNA sequencing. [2-5] Advances in single-molecule microscopy make it possible to observe reactions on the molecular level, rather than obtaining ensemble-based information. DNA sequencing and high-throughput screening of pathogen can be made faster and more cost-effective than ever with single-molecule microscopy. However, traditional imaging approaches are restricted by the diffraction-limited situation encountered in the confocal microscope or other far-field optics. In these approaches, the diameter of an illuminated spot is approximately 250 nm, giving an excited volume of about 1 femtoliter. To hold only one molecule in this detection volume, the concentration of fluorescent molecules needs to be diluted to 2 nM or lower (**Fig. 1.1**). However, at very low concentrations (pM range), the detection of small number of molecules is time consuming and generally impractical because of very low signal-to-noise ratio. On the other hand, most biological reactions occur at orders of magnitude higher concentrations (typically μM). For example, protein-DNA reaction has a dissociation constant (K_D) in the micromolar range. Michaelis–Menten constant (K_M) of most enzymatic reaction lies in the micro to millimolar range. A much lower concentration of substrates can only generate little products, whose weak signals may be overshadowed by signals from unreacted substrates.

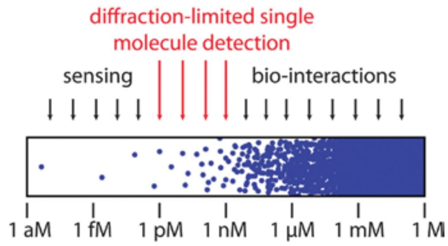

Figure 1.1 Typical concentration range of single-molecule experiments and bio-reaction. Reproduced with permission from Ref. [6]

To tackle this issue, a natural idea is to reduce the observation volume in order to reach higher concentration. For example, if the volume of interest reduces to the order of 10^{-4}fL (10^{-19}L), the upper concentration can reach 10 μM. In this case the dimension of this observation volume is in the order of tens of nanometers. If we can enhance the light-matter interaction in this volume, high signal-to-noise ratio result can be generated. Fortunately, developments in nanophotonics and nanoplasmonics show that nanoaperture in a metal film is an ideal structure to reduce observation volume and enhance light-matter interaction at the same time. In the next part we will briefly discuss the principles of nanoplasmonics and enhanced light-matter interaction.

1.2 Principles of nanoplasmonics and applications in fluorescence enhancement

1.2.1 Surface plasmon resonance (SPR)

Surface plasmon resonance (SPR) is the interaction between conduction electrons and incident light at the interface of conductive metal and dielectric material, which is often observed in nanostructures or nanoparticles made of noble metal like gold or silver. SPRs are collective electronic oscillations generated in this process. They can be categorized into two classes: propagating surface plasmon resonance (PSPR) and localized surface plasmon resonance (LSPR). [7] Along the metal-dielectric interface, surface plasma polariton (SPP) travels with an exponentially decaying intensity in the direction perpendicular to the surface. In this way, most of the energy is confined to the surface. Localized surface plasmon resonance (LSPR) is generated by metal nanoparticles, typically gold or silver, as compared to a continuous film of noble metal in traditional propagational SPR. Compared to typical decay length of 250-1000nm in PSPR, smaller decay length of evanescent field in LSPR (20-40nm) makes it less sensitive to bulky effect such as concentration or temperature fluctuation. This means LSPR is more sensitive to binding effect which happen on the surface of nanoparticle. LSPR is highly sensitive to the change in local refractive index. A shift in resonance wavelength ($\Delta\lambda$) indicates the binding event(s) of molecules. LSPR effect is less dependent on the angle between incident light and surface compared with PSPR. Based on this property, most LSPR based sensing devices feature transmission configuration. Below is a comparison in sensing principles between PSPR and LSPR sensors. (**Fig. 1.2**)

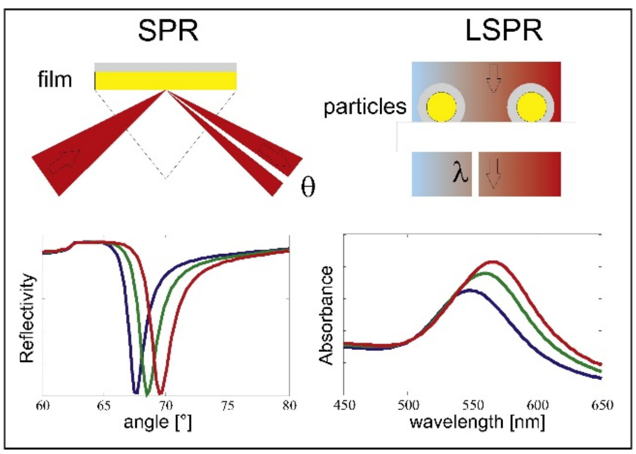

Figure 1.2 Schematics of the sensing principles for the studied PSPR and LSPR sensors. Reproduced with permission from Ref. [8].

1.2.2 Nanohole and nanohole-enhanced fluorescence

1.2.2.1 Nanohole and zero-mode waveguide (ZMW)

As is shown in our previous discussion, reducing observation volume is an effective way to achieve single-molecule detection at higher concentration. Previous approaches, including total internal reflective fluorescence microscopy (TIRF) [9] and near-field scanning optical microscopy (NSOM) [10] have been demonstrated to reduce the observation volume by creating evanescent field in a small, sub-diffraction volume. Another way to reduce the observation volume is to confine the excitation and detection volume in a small nanohole called zero-mode waveguide (ZMW). A ZMW can be simply fabricated by drilling a subwavelength nanohole (typically 50-200nm in diameter) on the metal-cladding glass slide. ZMW exhibits a cutoff wavelength (λ_c), above which no propagating mode exists. This also gives the name of "zero-mode" waveguide. The cutoff wavelength is related to the shape and size of waveguide. For longer wavelength above λ_c (λ >1.67 λ_c), an evanescent field will be generated and thus a small excitation volume in zeptoliter can be obtained. [11] Sketch of an aluminum ZMW and the electric field intensity distribution inside it is shown below. (**Fig. 1.3**)

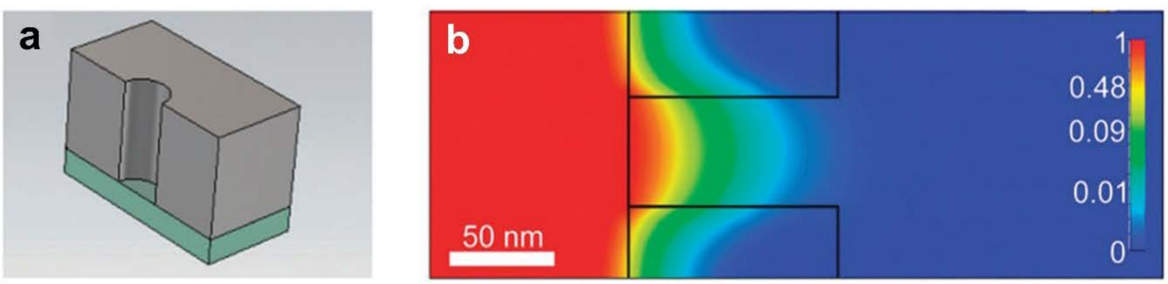

Figure. 1.3 Shape and optical properties of zero mode waveguide. (a)An aluminum ZMW with a diameter of 50nm and a width of 100nm on the glass substrate (b) Numerical simulation of the electric field intensity in the ZMW structure with of 500 nm incident wavelength coming from the left. Reproduced with permission from Ref. [11]

1.2.2.2 Nanohole-enhanced fluorescence and nanoantenna

Because of the plasmonic effect, nanohole array on noble metals convert propagating radiation into localized energy with enhanced local electromagnetic field. These electromagnetic field concentrated areas are usually referred to plasmonic "hotspots". As a result, enhanced fluorescence can be observed if spectral overlap appears between plasmonic resonance spectrum and fluorescence spectrum. The fluorescence enhancement factor can be defined as:

$$\eta_F = \frac{Q^*}{Q} = \frac{\kappa^*}{\kappa}\frac{\varphi^*}{\varphi}\frac{I^*_{exc}}{I_{exc}}$$

Where Q refers to brightness per emitter, κ refers to collection efficiency of an optical microscope, Φ refers to fluorescence quantum yield and I_{exc} refers to excitation intensity. [12] Physical quantities with star refers to enhanced properties in the expression. The collection efficiency and excitation intensity can be locally enhanced because of enhanced local electric field. The quantum yield Φ, can be modified by the coupling between the plasmon and the fluorophore that changes both the radiative and nonradiative rate of the complex. For fluorescent dyes with a relatively low quantum yield (several percent), enhancement would be much larger than those with higher quantum yield. [12] This can be partly understood by the fact that it is easier to reduce non-radiative energy loss for low quantum yield fluorophore than higher ones. It is also worth noting that opposed to enhanced fluorescence, fluorophore near metallic surface may also exhibit quenching effect in a distance less than a few nanometers. [13]

A step forward toward higher enhancement of fluorescence with plasmonic structure is well-designed nanoantenna. Nanoantennas are plasmonic structures with sharp curvature radii or nanoscale gaps and exhibit strong localized SPR property. It works in a similar manner to microwave and radio wave receiving antenna, which focus disperse and low-intensity electromagnetic wave into localized energy. In nanoantenna, the free electrons are forced to oscillate collectively under external illumination. This leads to strong focusing of optical field in a small area (the hotspot), where fluorescence can be greatly enhanced locally. Geometry of nanoantenna, like curvature and gap size, has strong influence on the performance of fluorescence enhancement. [14] Nanoantennas can be fabricated with either top-down method like focused ion beam [15] or electron beam lithography[16, 17], or bottom-up self-assembly method like DNA origami. [18] With bowtie shaped nanoantenna, the fluorescence enhancement factor of 1340 has been reported. [17] To reach single-molecule detection in micromolar concentrations, an “antenna-in-box” design was reported. In this design, two 76 nm hemispheres with 10-40 nm gaps were used for fluorescence enhancement, while a surrounding rectangular nanoaperture rejects the background signal. [15] Representative nanoantenna with strong fluorescence enhancements are summarized below. **(Fig. 1.4)**

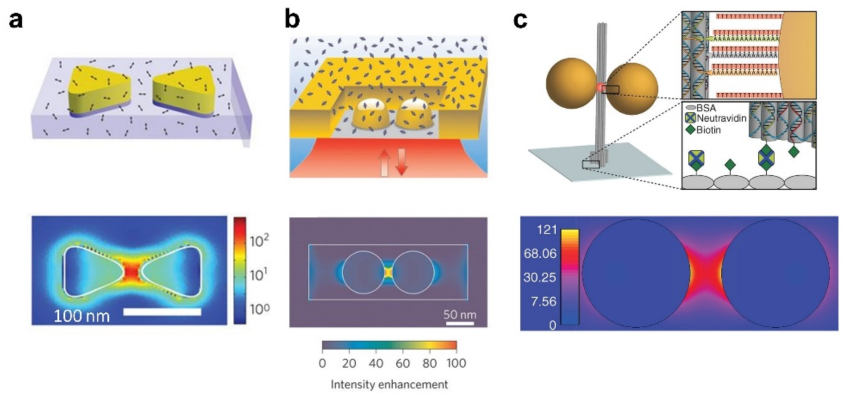

Figure 1.4. Nanoantennas for fluorescence enhancement. (a)Bowtie shaped nanoantenna covered by fluorescent molecules fixed in PMMA resin. [17] (b) “Antenna-in-box” nanoantenna with maximum for single-molecule detection at micromolar concentration. [15] (c) Nanoantenna assembled from DNA origami structures with nanogaps. [18] Reproduced with permission from Ref. [15, 17, 18]

1.3 Mobile phone imaging and nano-sensing

1.3.1 Overview of mobile phone imaging

Although conventional benchtop microscopes are still predominant in biomedical imaging, hand-held cellphone imaging device has gained increasing attention as an emerging imaging instrument. Compared to their bulky and costly counterparts, cellphone-based imaging devices are light weight, field-deployable, cost-effective, and easy to use. Cellphone imaging devices have shown great potential in point-of-care (POC) testing, where sample collection, testing, and reporting happen at the time and place of patient care. Optical methods are easy to implement on cellphone devices by integrating cost-effective optical components. Technological advance in cellphone cameras and image sensors has also made it possible to achieve high resolution and sensitivity on cellphone imaging devices. Especially for resource-limited areas, cellphone-based imaging and sensing devices can potentially achieve wide applications as a substitute for traditional benchtop instruments. [19]

Hardware configuration is the basis for the performance and capability of smartphone, most-importantly the camera on the smartphone. A smartphone camera consists of lens system to collect light and image sensor to convert optical signal into electronic signal. The smartphone cameras have undergone massive technological advances. In the past decade, the total pixel count of smartphone image sensor chips doubles almost every two years, following a Moore's Law trend. [20] High-performance image sensors have been applied to the newest smartphone models, producing much better-quality images than before. As of July 2018, smartphone-based CMOS image sensors (e.g., Sony IMX 586) provide pixel counts as high as 48 megapixel and pixel size as small as 0.8 μm.[21] As a result, the optical resolution of a smartphone microscope can be enhanced theoretically to the micron level. In terms of the sensitivity, smartphone image sensors with pixel size of 1.55 μm has been released. [22] In addition, powerful processors and adequate memory have made it possible to process and store data directly on the phone.

1.3.2 Attempts towards single-molecule imaging on a mobile phone

A number of trials have been made towards pushing the sensitivity of mobile phones from single nanoparticle to quantified number of fluorophores per diffraction limited spot. (**Fig.**

1.5) Fluorescence imaging have been adopted in these trials, which features low background signal and high signal-to-noise ratio compared to other imaging modalities. Single nanoparticles, single virus and single DNA molecule have been successfully imaged on the smartphone microscopy platforms, demonstrating the feasibility of nanoscale sensing on the smartphone. [23, 24] With plasmonic enhanced smartphone fluorescence microscopy, DNA origami nanoparticles were detected on the smartphone. In this work, a thin layer of 30-50 nm silver was coated on the glass coverslip and further coated with silicon dioxide to prevent quenching of fluorophores. Due to the plasmonic enhancement of silver layer, nanoparticles with 80 fluorophores were detected on the smartphone. [25] Most recently, detection limit of fluorophores per detection limit spots have reached 10 fluorophores by using a sensitive, monochromic image sensor, being the state-of-art result towards single molecule imaging on a smartphone. [26]

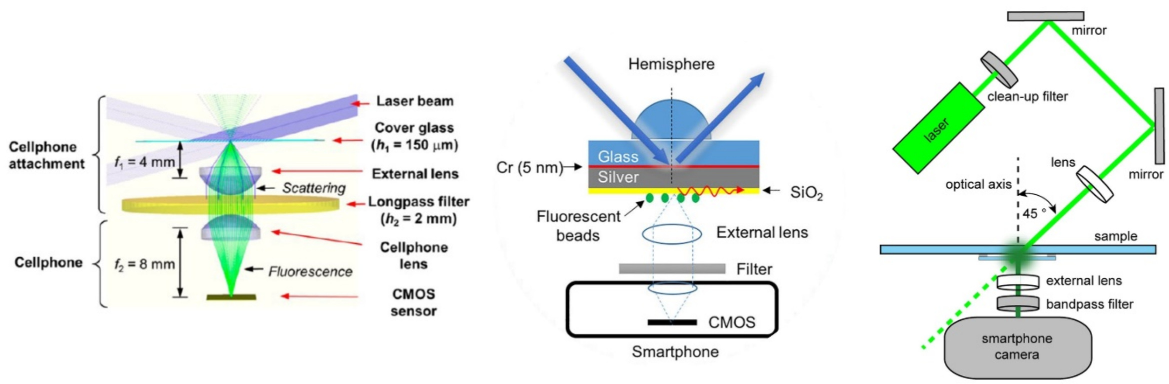

Figure 1.5 Optical setup in smartphone fluorescence microscopy toward single-molecule sensitivity. (a) Smartphone fluorescence microscope for single nanoparticle and single virus particle. (b) Plasmonics enhanced smartphone fluorescence microscope. (c) Optical setup and imaging results of detecting 10 fluorophores per diffraction limited spot. Reproduced with permission from Ref. [23] [25, 26]

1.3.3 Challenges of single molecule imaging on a mobile phone

Despite the attempts towards single-molecule sensitivity on a mobile phone, insufficient sensitivity and high background signal are still the main issue toward this goal. Single-fluorophore sensitivity have only been demonstrated and well-studied on large scale image sensor such as electron-multiplying charge-coupled device (EMCCD) or scientific CMOS (sCMOS) image sensor, which are used on the cameras of benchtop microscopes. Even the most sensitive smartphone image sensor on the market cannot reach this goal. High imaging background is another obstacle which impair the signal-to-background ratio. Most smartphone cameras have lens system with small focal distance and large aperture (large f number, f/#) for larger field of view and better performance at dark environments. This gives a small value numerical aperture (NA), which is defined as:

$$NA = nsin\alpha \approx \frac{n}{2(f/\#)}$$

where n is the refractive index of the medium, α is the half angle of the cone of light exiting the lens pupil, and f number is defined as *f/# = f/D*, in which f is the focal length and D is the entrance pupil diameter of the lens system. In fluorescence imaging, low numerical aperture is related to low signal-to-background ratio (SBR). SBR from stray light background scales with four times of NA and SBR from unfiltered specular reflectance scales with twice of NA. [27] Typically, a smartphone camera has NA around 0.2, while objective lens on benchtop microscope can reach NA of 0.6 for dry objectives and even 1.25 - 1.4 for oil immersion objective. Solving these problems are important to achieve single molecule imaging on the smartphone.

1.4 Motivation

Smartphone has proved its potential in health monitoring and disease diagnostics by the detection of low concentration biomarkers and nucleic acids. To further exploit the potential of smartphone application in biomedical detection, a single-molecule sensitivity is the ultimate goal. With single-molecule sensitivity, a number of applications of single molecule imaging including DNA sequencing can be carried out on a mobile phone. Single molecule sensitivity on a mobile phone sensor would also be a milestone in portable nanosensing. Single molecule detection limit on a portable device would provide more opportunity in democratizing nanosensing tool to the public, which are traditionally only available in well-established centralized labs. Based on the the discussion above, our primary motivation is to utilize the fluorescence enhancement property from nanohole and background suppression property in zero-mode waveguide. We are aiming to observe combined effect of these two properties in nanohole array on gold surface.

CHAPTER 2: Single-molecule imaging test on a benchtop microscope via nanohole enhanced fluorescence.

2.1. Introduction

Mobile phone imaging of single molecule provides promising application in point of care detection of protein or nucleic acid with very low concentration. Yet to achieve single molecule imaging on a mobile phone, the fluorescence signal has to be amplified to increase the signal-to-noise ratio and allow the fluorescence signal to be strong enough to be detected by the imaging sensor on the phone. In recent years, plasmonic structures have been studied extensively in the enhancement of fluorescence signal. Nanohole, which is a nanoscale aperture milled in the thin film of plasmonic metal, is a representative and well-studied nanostructure in fluorescence enhancement. Gold nanohole is the most commonly studied and is used in this work. Due to the property called surface plasmon resonance, gold nanohole is capable of enhancing local electric field when incident light with certain range of wavelength is present. The locally enhanced excitation field is the main contribution to the enhancement of the fluorescence signal. In this application, the ability to enhance fluorescence, which is often referred to as “enhancement factor”, is crucial of demonstrating the concept of single molecule imaging on the smartphone. Currently, the closest attempt towards single molecule imaging on a mobile phone is the ability to detect 10 fluorophores per diffraction limited spot. [26] If 10 times florescence enhancement can be achieved with nanohole substrate, single molecule sensitivity could be possibly achieved on the smartphone. Similar to other plasmonic nanostructures such as gold nanoparticle, the SPR property of gold nanohole is highly dependent on its geometric dimensions. To reach over 10 times enhancement, both the hole size and film thickness are crucial parameters that determine the performance of fluorescence enhancement. In this sense, the geometric parameters of nanohole substrates used for fluorescence enhancement should be rationally controlled. For gold nanoholes, both the thickness of gold film and diameter of nanohole has significant influence on the fluorescence enhancement performance of gold nanohole array. [28-32] Within the nanohole, the field enhancement is also dependent on local curvature radii. Those regions with small curvature radii are called “hot spots”. In a nanohole, hot spots are located at the edge on both bottom plane and top plane.Based on the reported results, we are trying to optimize the hole size and thickness to achieve larger than 10 times enhancement of fluorescence on the nanohole substrate. Distance between two holes (or period) also has influence on the SPR peak intensity and position. Smaller period can cause blue shift of SPR peak position and increase the intensity of SPR peak. [29] Yet if the period is too small, it might pose some difficulty for optical resolution of two adjacent holes. The period was set to be 2μm in the preliminary tests.

Another important issue is the selection of dye in the test. From previous research, plasmonic peaks of gold nanohole structure lies primarily between 600-1000 nm. [29, 31, 33] For the optimal choice of dye, the excitation and/or emission peaks should overlap with those plasmonic peaks for maximizing harvest of the locally enhanced electric field. On the other hand, to meet our goal of single molecule imaging on a mobile phone, the emission of the dye molecule should be strong enough to be detected within the dynamic range of RGB sensor of the smartphone. For most smartphone sensors, the presence of the on-chip color filters and IR has made the smartphone image sensor much less sensitive above 650 nm. [34, 35] Among fluorescent dyes with emission less than 650 nm, Alexa Fluor® 633 was chosen, which is a widely-used fluorescent labelling fluorophore in biological research with excitation/emission peaks at 632/647 nm. From the discussion above, the plasmonic peaks of nanohole should also cover the excitation and/or the emission peak as much as possible. Gold films with 100 nm thickness and hole size varying from 100 nm to 200 nm in diameter were first tested in the experiment.

2.2. Material and methods.

2.2.1 Nanohole array substrate fabrication and characterization

Glass coverslip (no. 1, Fischerbrand) was rinsed in piranha solution for 30 minutes to remove organic residue on the surface. After dried with compressed nitrogen, 5 nm of titanium and 100 nm of gold was deposited on the glass using DC sputtering. Nanohole patterning was performed using focused ion beam (FIB) on a FEI quanta 3D dual beam with 30kV acceleration voltage, 10 pA beam current and 10μs dwell time. The depth of nanoholes were set to be 100nm and diameters were set in the range of 100 nm to 200 nm. Scanning electron microscopy (SEM) images were taken on the same instrument using electron beam. To measure the depth of the nanohole, a small patch of platinum (1.5 μm × 1.5 μm × 200 nm) was deposited over a nanohole to fill the nanohole completely. A cross-section at the diameter of the nanohole was made subsequently. The depth of a nanohole can be measured by observing the contrast between platinum, gold and glass. Overall the depth of nanoholes with inputted parameter were measured to be 101 nm.

2.2.2 Single molecule imaging on benchtop microscope

Single molecule imaging was tested on Olympus IX 83 inverted microscope. To start with, untreated glass coverslips were rinsed with acetone, isopropanol and methanol to remove organic impurities. Fluorescent dye Alexa 633 (carboxylic acid, Thermo Fischer) was dissolved in PBS buffer and further diluted to working concentration ranging from 1 μM to 30 nM. Each time 1 μL solution was drop casted onto the glass substrate to form a circular region containing dye molecules. The glass coverslip was imaged under 100x oil immersion lens (Olympus, NA=1.40) in Cy5 channel. The blinking video was recorded with an exposure time of 500 ms and frame rate of 1 fps. Typically, 300-500 frames were recorded in a video. Test on the nanohole substrates followed the same sample cleaning and preparation method. The image sequence was subsequently processed with ImageJ, an open-source software for image processing.

2.3. Results

2.3.1. Nanofabrication and characterization of gold nanohole substrate

Nanofabrication of gold nanohole was achieved by physical deposition of gold via DC sputtering and nanoscale cutting enabled by focused ion beam, a commonly used technique in nanofabrication. DC sputtering is a low-cost and simple way in metallic thin film deposition. The thickness can be controlled by setting deposition time and current. To increase the adhesion between gold and glass, 5 nm of titanium was first deposited on the glass as the adhesion layer. 100 nm of gold was deposited subsequently. The next step is to fabricate nanohole on the gold surface. Focused ion beam (FIB) was adopted as it has been applied many times in fabricating nanohole array for fluorescence enhancement. [7, 36, 37] Inside a FIB instrument, accelerated gallium (Ga) ion was focused with electromagnetic lens and sputtered onto the surface to remove material. The resolution of the beam can be as low as a few nanometers, so it’s capable of fabricating nanohole with diameter of a few hundred of nanometers. The depth of the nanohole can be controlled both by inputted Z size and dwell time of the beam. The sample can be also imaged on the same instrument with electron beam. A representative SEM image of 150 nm nanohole array is shown in Figure 2.1 (a). To precisely measure the depth of the nanohole, the depth of the nanohole was also measured by platinum (Pt) deposition on the same instrument. By filling the hole with platinum and cut a cross-section at the diameter of a nanohole, we can observe the actual depth of the nanohole. Both schematic illustration and SEM image of nanohole cross section is shown in Figure 2.1 (b), (c). A linear relationship between inputted depth parameter and actual depth is summarized in Figure 2.1 (d) We can find that the nanohole is not perfectly shaped in a cylinder, but rather to be a conical shape. This is an intrinsic property of FIB fabrication, due to the non-perfect, Gaussian beam profile that made the sidewall oblique rather than upright. [38] The size of the beam should also be taken into account. Patterning was achieved by manually entering the coordinates of each hole. Nanohole arrays with 100 nm, 150 nm and 200 nm were fabricated with the same way. The total time took to fabricate 400 holes ranged between 1 min to 5 min, making it a rather efficient way to fabricate large amount of nanoholes.

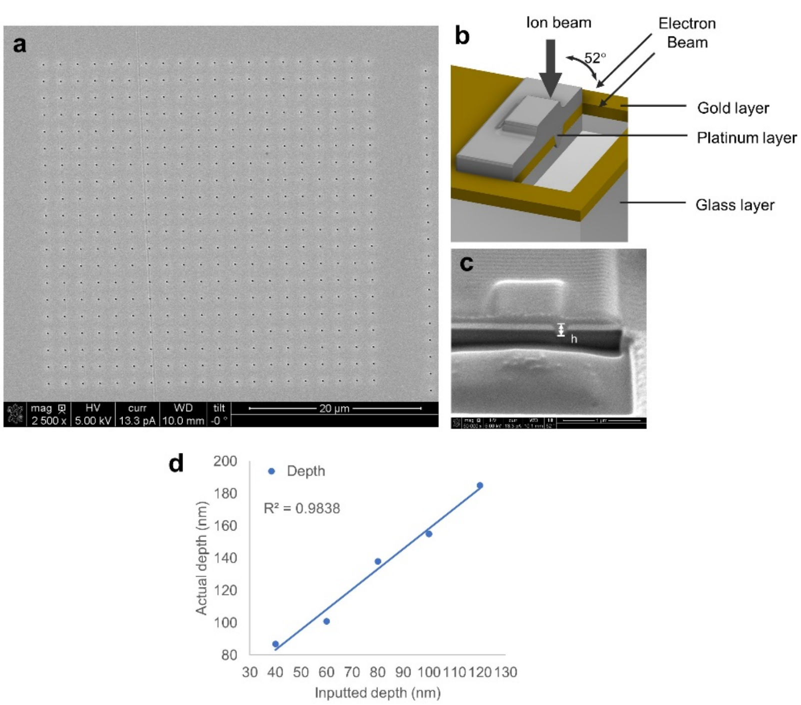

Figure 2.1 Fabrication and characterization of nanohole array. (a)Electron beam image of 20×20 nanohole array with 150 nm diameter and 2 μm period. (b) Schematic illustration of depth measurement (c) SEM image of the cross-section made during depth measurement, showing the depth of the nanohole. (d) Depth measurement of FIB fabricated nanohole by Pt deposition.

2.3.2. Single molecule imaging on benchtop microscope and enhancement calculation

The benchtop test serves as preliminary experiments before imaging single molecule on mobile phone. With well-established optical systems and sensitive scientific CMOS (sCMOS) camera, typical single molecule blinking and photobleach behavior are expected to be observed in this, as well as to quantify the fluorescence enhancement factor (EF) on nanohole substrate. To observe single molecule behavior, the dye concentration has to be rather low to allow single molecule fluorescence signal be observed. Before the nanohole substrate was tested, single molecule imaging was tested on blank glass coverslip for comparison. This allow us to observe unenhanced single molecule behavior by plotting the pixel intensity of a bright spot over time. A typical image of single molecule imaging result and a single molecule blinking time trace on the glass slide was shown as in Figure 2.2. Each fluorescent dye molecule will be photobleached eventually, given enough illumination time. Before it's photobleached, it may absorb photon to jump to excited state and returning to the ground state, which is reflected by the blinking behavior. The step on the single molecule time trace can reflect fluorescence intensity of a single fluorophore. From the number of the steps, the number of fluorophores observed can be obtained. It could be observed that in Figure 2.2 (b), only one dye molecule was placed at the spot of interest. While in Figure 2.2 (c), two dye molecules were placed at the spot of interest, which were photobleached one after another. For both time traces, similar photobleaching step was observed, indicating single-molecule photobleaching behavior was detected. Step size was calculated to reflect fluorescence intensity for each fluorophore.

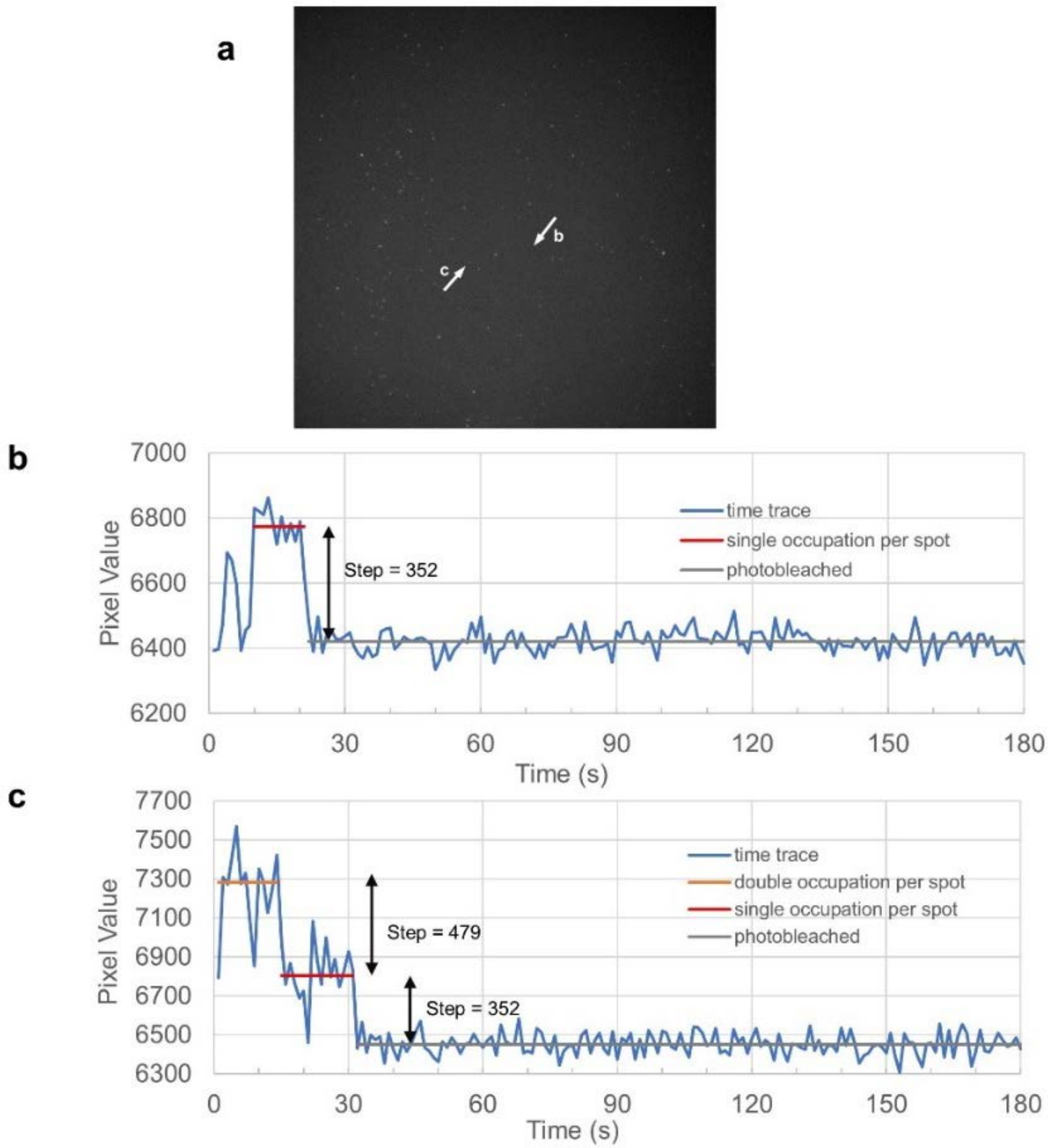

Figure 2.2 Single molecule blinking and photobleaching on blank glass substrate. (a) The first frame of the image sequence captured on benchtop microscope. The dye solution was diluted to 50 nM and 1 μL solution was added to the glass coverslip and allowed to dry. Brightness of image was adjusted to show the fluorescence signal from dye molecules. (b) Single-molecule blinking time trace at the point marked by arrow b in panel (a). (c) Single-molecule blinking time trace at the point marked by arrow c in panel (a).

To image enhanced fluorescence and calculate enhancement factor, single molecule imaging experiment was also carried out on nanohole substrates. Figure 2.3 shows single-molecule experiment on 100 nm substrate. The optical image captured in bright field mode in Figure 2.3 (a) shows the nanohole is visible under microscope. The bright stripes on the image was made on purpose as mark during FIB fabrication. Fluorescence monochromic image from the image sequence (Figure 3(b)) shows that most of the spots lies within the nanohole, because fluorescence from the molecules that lie out of the nanohole would be quenched by the gold surface. However, some bright spots are still visible outside the nanohole, which might be the result of surface impurities that absorb dye molecules. By plotting the pixel value to time, time trace for two spots were obtained which were shown in Figure 2.3 (c) and (d). Blinking and photobleaching can be observed from the time traces. Two steps can be observed from Fig. 2.3 (d) which indicates double occupation of dye molecules per spot. The step size was also calculated, yet smaller than the step size on the nanohole surface is slightly smaller than the step size on glass surface. Given the step sizes, the enhancement factor was supposed to be calculated as followed:

$$\eta = \frac{Step_{nanohole}}{Step_{glass}}$$

This gives us an enhancement factor of 0.85, which is smaller than one. More discussions about this result will be made in the discussion section.

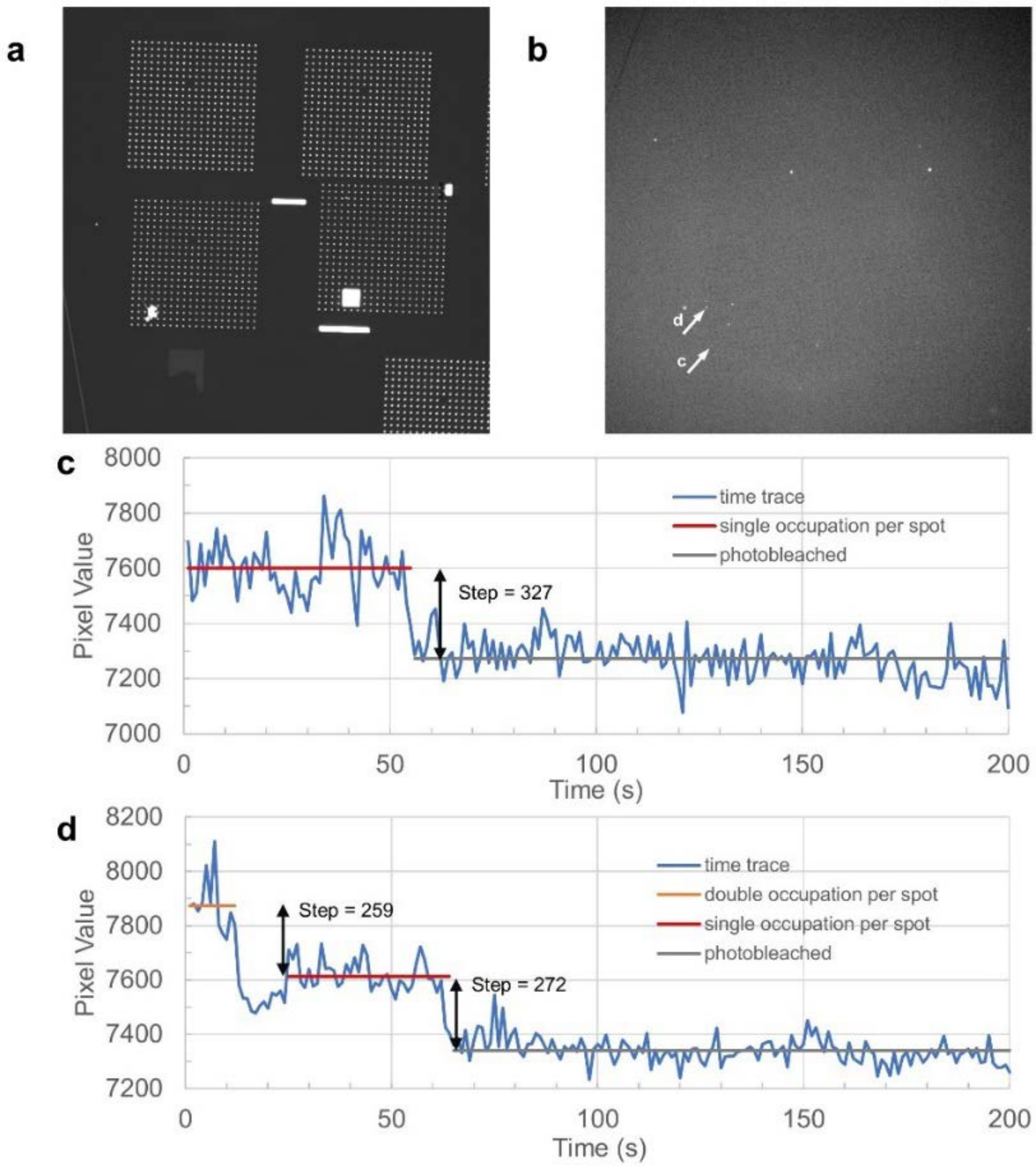

Figure 2.3 Single molecule blinking and photobleaching on 100 nm nanohole. (a) Bright field image of 100 nm nanohole array. (b) The first frame of the image sequence captured on benchtop microscope. Sample preparation method was the same with glass sample. Brightness of image was adjusted to show the fluorescence signal from dye molecules. (c) Single-molecule blinking time trace at the point marked by arrow c in panel (b). (d) Single-molecule blinking time trace at the point marked by arrow d in panel (b).

2.4. Discussions and future steps.

A number of variables in the experiment can lead to inaccurate result of calculated enhancement factor. First, in the nanofabrication step, the nanohole is not perfectly cylinder shaped. As surface curvature is important in the simulation in fluorescence enhancement from nanostructures, this might add some discrepancies with the theoretical model and experimental results. In future nanofabrication experiments, we will use smaller beam current which gives narrower beam profile. The position of the dye molecule inside the nanohole also added uncertainty to the result. In our experiment the dye molecules are randomly placed inside the nanohole. From the simulation, only the molecules at the very proximity of the sidewall have maximum enhancement of fluorescence. If the molecule is placed at the center, enhancement might not be as strong as maximum enhancement. Meanwhile, the amount of dye molecules inside the nanohole is not large enough for large-scale analysis. Some surface chemistry and bioconjugation test can be added to future plans in order to deliver the fluorescent dye molecule inside the nanohole. The temporal resolution makes the experiment challenging on the current setup as well. In some literatures, frame rate as fast as 10 fps was used. [17, 39] This is 10 times to our current experiment setup, which give 10 times more information to be analyzed. The hardware setup could be updated in the future to help us better understand the single molecule behavior by collecting more data points.

CHAPTER 3. Development of modular and dual-functional smartphone microscopy platform – EpiView (A part of a collaboration project with Duke University)

3.1 Introduction

Recent advances in telemedicine, mobile microscopy, computational imaging, and point-of-care (POC) technology have opened new possibilities for democratizing access to diagnostic modalities that might otherwise be unavailable in low resource setting (LRS). By leveraging the portability, cost-effectiveness, computing power, and digital sensing capabilities of mobile platforms, these innovations have shown promising performance in clinical settings, including in LRS. These devices were shown to capture images comparable to those obtained with a conventional light microscope for histopathology and IHC specimens, and in some cases could automate digital processing and readout. Furthermore, mobile platforms are capable of wireless connectivity. Widespread access to the internet and availability of cellular networks (even in in LRS) presents the possibility of wirelessly transmitting digital results to remote providers offsite who can interpret results and triage cases. Yet to date these technologies have mainly been applied toward cell block-based preparations (histopathology and IHC), which are dependent on access to sophisticated tools for sample preparation (e.g. CNB, fixation, embedding, sectioning). Taken together, the availability of a portable and user-friendly approach based on FNA sampling that is capable of (1) assessing cellular pathology (via cytology) and (2) credentialing molecular biomarker status on a single, low-cost platform would represent a powerful tool in the armamentarium against BC worldwide, particularly where resources are scarce.

Herein we demonstrate our attempt at addressing the challenges above, using a unified mobile pathology platform, the “EpiView-D4”. The device is designed to be operated in environments where basic FNA preparations are feasible. It accomplishes both cytology and molecular analysis of BC cellular aspirates on a single portable platform at reduced complexity and cost compared to standard laboratory methods. The EpiView-D4 is comprised of two components: an immunodiagnostic chip (the "D4") which quantifies expression of molecular biomarkers, plus a custom cellphone-based optical microscope (the "EpiView") that performs both brightfield imaging of basic cytology preparations and fluorescent readout of the D4 chip. First, we demonstrate that the D4 chip is capable of molecular credentialing of cultured BC cells. As proof-of-concept, in this paper we focus on applying the D4 chip toward quantifying expression levels of human epidermal growth factor receptor-2 (HER2), a well-established biomarker which carries prognostic value and is specifically targetable by drugs (i.e. trastuzumab). We next show the design and operational performance of the EpiView as a "dual-function" mobile microscopy platform for both brightfield (cytology) and fluorescence (D4) imaging. Combining these two elements as the EpiView-D4, we then apply the technology towards characterizing FNA specimens (both cytology and HER2 expression) from orthotopically engrafted models of human BC in mice. Finally, we extend the translational relevance of the EpiView-D4 to BC specimens taken from human patients in a pilot clinical study at Duke University Hospital. Taken together, these results suggest the EpiView-D4 might provide a potential first step toward expanding the breadth and accessibility of BC pathology services in LRS.

3.2 Material and methods

3.2.1 Design and preparation of the EpiView scope

The dual function smartphone microscope, EpiView, was comprised of 3D-printed optomechanical attachments and a Nokia Lumia 1020 smartphone. The 3D-printed attachments were designed by Autodesk Inventor and prepared by 3D printing (StrataSys uPrint SE plus), which include a base attachment to be mounted on the smartphone and two switchable imaging modules for different functions. Both imaging modules can be slid into the base attachment to form a standalone handheld device for brightfield or epifluorescence imaging applications, respectively. In the assembled brightfield device, a 1/2" dovetail translation focusing stage (DT12, Thorlabs) was mounted above the external lens for focusing adjustment. The imaging module contains a white LED (3.2 V, 897-1183-ND, Digikey) powered with a coin cell battery (CR2032) for illumination, a glass slide sample holder, and two pieces of filter paper as diffuser placed between the light source and the sample. A lens module (f_2 = 2.6 mm, UCTronics) was placed right in front of the smartphone camera as the objective. The smartphone carries an 2/3-inch, 38 megapixels (5360 × 7152) complementary metal-oxide semiconductor (CMOS) image sensor. The lens on the smartphone camera has a focal length of f_1 = 6.86 mm. Therefore, the magnification of the brightfield imaging system can be calculated: $M = f_1/f_2 \approx 2.6$mm.

In the epifluorescence modality, a green laser diode (532nm, <150mW, Z-bolt) powered by 2 AA batteries was connected with a heatsink and mounted together on the base attachment. The laser beam was expanded by a beam-expander module comprised of a concave lens (f_3 = -9 mm, #84-378, Edmund Optics) and a convex lens (f_4 = 24 mm, #65-480, Edmund Optics) which together give a magnifying power MF = -f4/f3 ≈ 2.6 x. After passing the beam focusing lens (f_5 = 15 mm, #69-387, Edmund Optics) the beam was deflected by 90 degrees by a dichroic mirror with the cut-on wavelength of 552 nm (#34-736, Edmund Optics). The beam was focused again by an objective lens module ($f_6 \approx$ 8mm, DTR's laser shop) before reaching the sample. A 585 nm band-pass filter was placed in front of the smartphone camera as an emission filter to collect fluorescence from the sample. A micro focusing stage and a sample holder were also placed in the imaging module similar to the brightfield attachment. A cell-battery powered white LED (3.2 V, 897-1183-ND, Digikey) used as light source for pre-focusing.

3.2.2 Image acquisition with EpiView and data analysis

The brightfield imaging was performed on EpiView to capture the images of both FNA and HER2-IHC slides. To do so, a sample slide was inserted to the sample holder of the brightfield imaging module, followed by turn-on of LED and focusing. The built-in smartphone camera app (Nokia Camera Pro) was used for digital image acquisition. An integration time of 0.4 second and an ISO value of 200 was used for both FNA slides and HER2-IHC slide. All the images were stored as lossless format (DNG file), which can be converted to TIFF file for further analysis with ImageJ or Matlab.

Smartphone fluorescence imaging was performed on EpiView to quantify the intensity of D4 microarrrays, which were designed and printed by our collaborator. To test the sensitivity of fluorescence mode, red polystyrene microspheres (FluoSpheres™, 580 nm/605 nm, ThermoFischer) with diameters ranging from 1 μm to 200 nm were used. Suspension of fluorescent microsphere was diluted 5,000 – 1,000,000 times depending on the size of the microsphere for desired density of microspheres in a field of view. The glass coverslip was rinsed with acetone, isopropanol, and methanol, blow-dried, and finally treated with plasma for a few seconds. 1 μL diluted microsphere suspension was added to the coverslip and dried in air. The sample was then inserted into the coverslip holder of the fluorescence module for imaging. The white LED was first used to focus the sample before the laser was turned on to minimize photobleaching and laser overheating. In the imaging of 200 nm microspheres, an integration time of 2 seconds and an ISO value of 400 was used. To validate single nanoparticle imaging, the same fluorescent nanoparticle sample used in the sensitivity test was also imaged by a benchtop inverted microscope (Olympus IX83). The fluorescent sample was imaged by using a 40x objective lens (NA = 0.60) of the same area imaged by the smartphone microscope. Digital images were acquired in Cy5 channel with an integration time of 1s by using a scientific CMOS camera (Hamamatsu Flash4.0).

A similar procedure was used for fluorescence imaging of the D4 assay chips. An integration time of 1s and an ISO value of 400 was used in imaging all D4 samples. To quantify the fluorescence intensity of D4 microarrays, the raw smartphone DNG images were first converted to the TIFF images, and then the green channel was extracted for intensity analysis. The average pixel intensity of the bright spots was measured using ImageJ.

To test the spatial resolution of EpiView, an USAF 1951 resolution test target was imaged with brightfield and epifluorescence imaging attachments (in brightfield mode), respectively. The resolution target was place between the white LED and the smartphone camera in both imaging attachment modules. The lossless raw DNG image was converted to TIFF image to extract the green channel for analysis.

3.3 Results.

Compliant and cost-effective optical reader devices capable of high analytical performance is a key element for POC diagnostics. Here, we developed a smartphone-based multimodal imaging platform, EpiView, which is able to quantify both fluorescent D4 assay chips and colorimetric FNA-derived cytology staining slides to address the need for measurement of various POC assays, rapid data analysis, and result storage or wireless transmission in LRS. The EpiView scope is constructed based on a new modular design, where two switchable imaging modules (one for brightfield and the other for fluorescence imaging) can be installed on a universal smartphone base attachment to support both high-performance brightfield and fluorescence imaging modalities. The base attachment only contains a laser diode and batteries for the fluorescence imaging modality.

The brightfield imaging module **(Fig. 3.1(a), (c))** features a transmission illumination design by using a white LED as the light source. The module also integrates a small translational micro-stage connected to the sample tray, an optical diffuser, and an external lens module for optical magnification. The fluorescence imaging module on the other side features an epifluorescence optical configuration **(Fig. 3.1(b), (d))**. In this design, a dichroic mirror placed 45 degrees to the incident light was used as beam splitter to deflect excitation light from a compact laser diode and allow emission light from the sample pass through to be collected by the smartphone camera. In addition to the focusing stage and optical filter, the imaging module also includes a conical beam expansion unit comprised of two singlet lenses to expand the diameter of laser beam by around 2.6x in order to fulfill the back aperture of the objective lens module. A white LED was also included for illumination during sample searching and initial focusing.

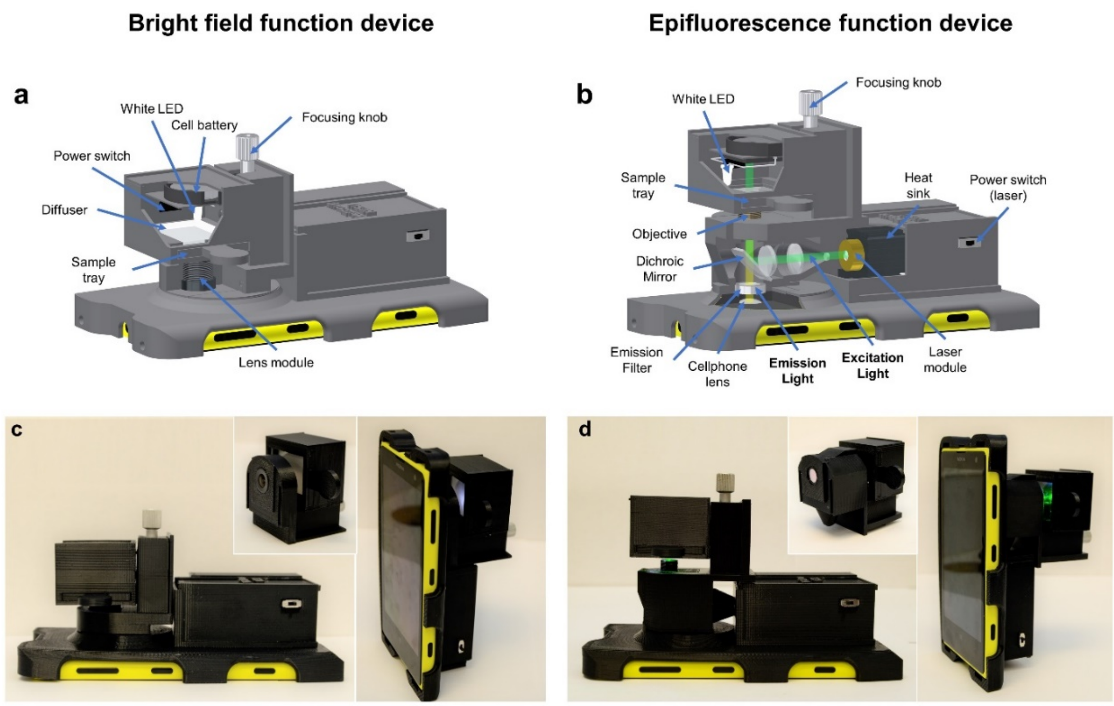

Figure 3.1 Optical configuration of EpiView. (a) 3D illustration of assembled bright field function device. (b) 3D illustration of assembled epifluorescence function device. (c) Photos of assembled bright field function device. (d) Photos of assembled epifluorescence function device.

To characterize the two attachments, resolution and field of view (FOV) was quantified on both devices. Most smartphone image sensors have on-chip color filter arrays called Bayer filter mosaics. In each unit there are two greens filters, one red filter and one blue filter. As a result, smartphone image sensor is typically most sensitive to the light within the range of green light. To accurately quantify the resolution, the green channel images were extracted from the RGB images of a USAF 1951 resolution test target captured on bright field modality and epifluorescence modality of EpiView. When installed on the smartphone base, the brightfield imaging module provides a spatial resolution of 1.1 μm **(Figure 3.2(a), (b))** and a field of view (FOV) of ~0.8 mm^2, which is sufficient for high-throughput and high-resolution imaging of FNA cytology and Her2-IHC slides. The fluorescence imaging module provides both a large FOV (~1.5 mm^2) and a fine lateral resolution of 2.6 μm **(Figure 3.2(c), (d))**. To demonstrate the detection sensitivity of the epifluorescence modality, 200-nm fluorescent polystyrene beads were imaged on this device **(Figure 3.2(e))**. The detection of single nanoparticles on the smartphone device was validated by comparison to benchtop microscope images obtained by a 40x objective. **(Figure 3.2(f))** Successful imaging of single, 200 nm nanoparticle on the epifluorescence device proved the comparable sensitivity with the state-of-art optical sensing devices on smartphone.

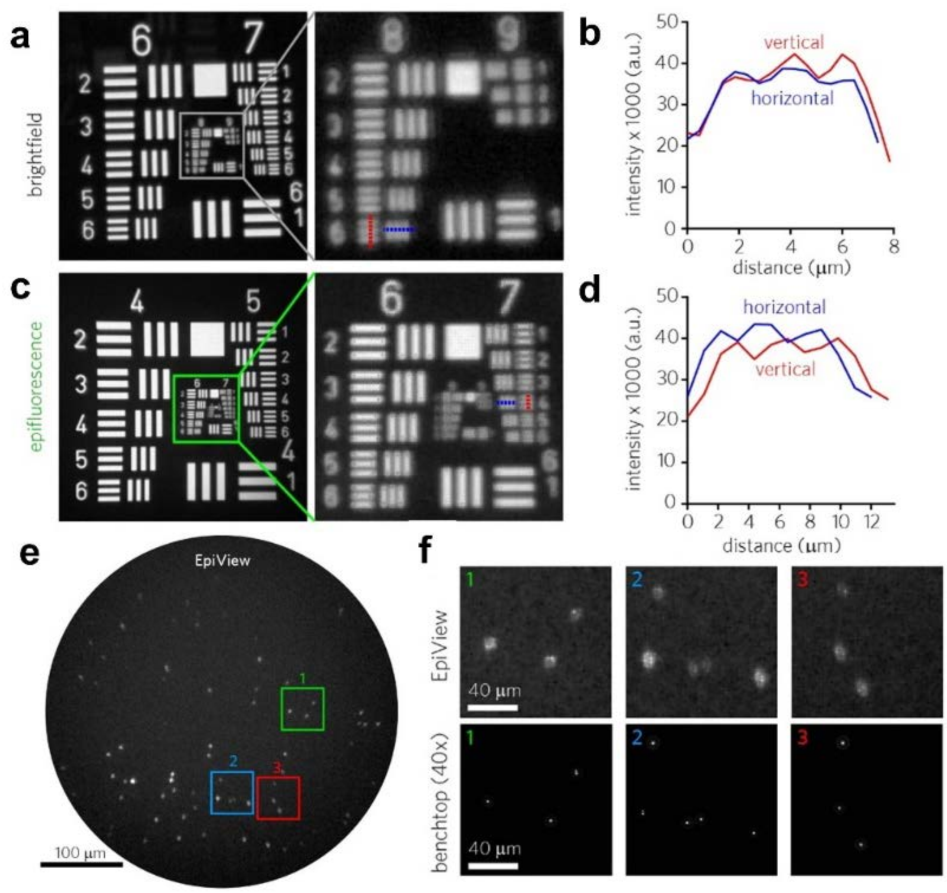

Figure 3.2 Characterization of EpiView. (a) Monochromic green channel image of a USAF 1951 resolution test target. (b) Intensity profile at dashed lines shown in (a). (c) Monochromic green channel image of the same resolution test target captured with epifluorescence modality of EpiView. (d) Intensity profile at dashed lines shown in (c).

To further improve the resolution of brightfield image, the point spread function (PSF) of the imaging system was measured and the raw brightfield images were deconvoluted in RGB color space (See details in the Materials and Methods section). After deconvolution, the spatial resolution was improved to 1 µm, and finer sub-cellular details and better image contrast can be observed in the FNA cytology slides (Fig. 3.3)

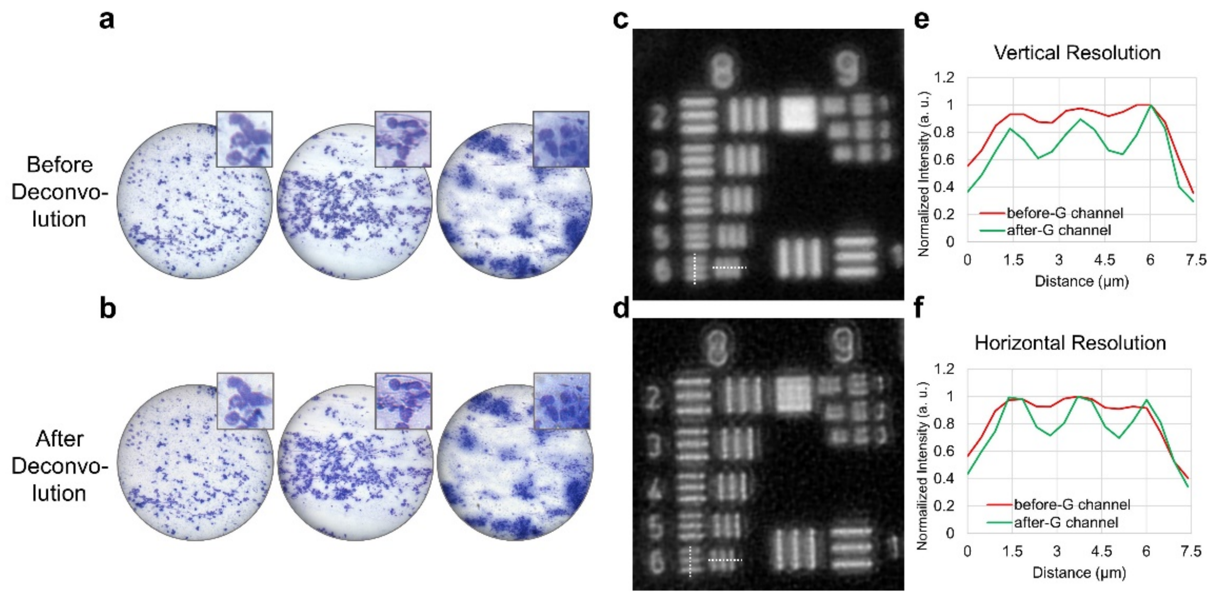

Figure 3.3 Bright field imaging and deconvolution. (a), (b) Bright field image of FNA slides before and after deconvolution. (c), (d) Bright field image of resolution test target slides before and after deconvolution. (e), (f) Improvement in vertical and horizontal resolution.

4. Discussions

In this work, we designed a dual-functional smartphone microscopy platform that is capable of bright field imaging and fluorescence imaging. The modular design makes it easier in switching between imaging modalities, making it possible to analyze the FNA pathological slide and the fluorescent D4 molecular assay on the same device. Despite its capability in breast cancer diagnostics and potentially diagnostic of other cancer, the epifluorescence configuration makes it free from dependence on imaging transparent sample. A number of potential applications including plasmonics enhanced molecular assay or surface fluorescence characterization could be achieved on this device in the future. This platform is also a promising candidate for nanohole enhanced fluorescence test on a mobile phone, and ultimately towards the goal of single molecule imaging on a portable mobile phone.

CHAPTER 4: Conclusions

4.1 Current achievements

In the single molecule imaging project, nanofabrication and benchtop tests have been carried out with some preliminary results. To enhance the fluorescence of dye molecules, gold nanohole arrays with thickness of 100 nm and diameter ranging from 100 nm to 200 nm have been fabricated and characterized. Characteristic single molecule fluorescence with blinking and photobleaching behavior have been observed on glass substrates and nanohole arrays by capturing image sequence on benchtop microscope. In the smartphone reader project, a smartphone microscopy platform with bright field imaging and fluorescent imaging functions have been designed, fabricated, characterized and tested with cytology slides. The epifluorescence part of the imaging platform can be applied as the smartphone detector for future single molecule imaging using plasmonic nanohole substrate on the phone.

4.2 Future works

In the single imaging project, a few more tests can be carried out in the near future. First, the strong fluorescence enhancement from was not observed. Due to the hydrophobic nature of gold film, aqueous sample cannot easily form uniform thin film on the gold nanohole substrate. This added some difficulty in sample preparation. The next goal is trying to improve the sample preparation method, by surface cleaning or adding polymer coating to modify the surface property of gold film. Second, temporal resolution of single-molecule time trace could be potentially improved by using more sensitive camera. If the fluorescence enhancement factor can be quantified, some surface chemistry experiments can be carried out to chemically immobilize fluorescent molecules in the nanohole. Supposedly this would increase the percentage of fluorescent molecules inside the nanohole, and high-throughput analysis of single molecule behavior could be made possible. Finally, the assay will be tested on the smartphone to validate the enhancement of fluorescence and ultimately achieve single molecule sensitivity on the smartphone.

References

[1] W.E. Moerner, L. Kador, Optical detection and spectroscopy of single molecules in a solid, Physical review letters 62(21) (1989) 2535.

[2] D.M. Rissin, C.W. Kan, T.G. Campbell, S.C. Howes, D.R. Fournier, L. Song, T. Piech, P.P. Patel, L. Chang, A.J. Rivnak, Single-molecule enzyme-linked immunosorbent assay detects serum proteins at subfemtomolar concentrations, Nature biotechnology 28(6) (2010) 595.

[3] L. Cohen, M.R. Hartman, A. Amardey-Wellington, D.R. Walt, Digital direct detection of microRNAs using single molecule arrays, Nucleic acids research 45(14) (2017) e137-e137.

[4] K.O. Nagata, C. Nakada, R.S. Kasai, A. Kusumi, K. Ueda, ABCA1 dimer–monomer interconversion during HDL generation revealed by single-molecule imaging, Proceedings of the National Academy of Sciences 110(13) (2013) 5034-5039.

[5] J. Eid, A. Fehr, J. Gray, K. Luong, J. Lyle, G. Otto, P. Peluso, D. Rank, P. Baybayan, B. Bettman, A. Bibillo, K. Bjornson, B. Chaudhuri, F. Christians, R. Cicero, S. Clark, R. Dalal, A. Dewinter, J. Dixon, M. Foquet, A. Gaertner, P. Hardenbol, C. Heiner, K. Hester, D. Holden, G. Kearns, X.X. Kong, R. Kuse, Y. Lacroix, S. Lin, P. Lundquist, C.C. Ma, P. Marks, M. Maxham, D. Murphy, I. Park, T. Pham, M. Phillips, J. Roy, R. Sebra, G. Shen, J. Sorenson, A. Tomaney, K. Travers, M. Trulson, J. Vieceli, J. Wegener, D. Wu, A. Yang, D. Zaccarin, P. Zhao, F. Zhong, J. Korlach, S. Turner, Real-Time DNA Sequencing from Single Polymerase Molecules, Science 323(5910) (2009) 133-138.

[6] P. Holzmeister, G.P. Acuna, D. Grohmann, P. Tinnefeld, Breaking the concentration limit of optical single-molecule detection, Chemical Society Reviews 43(4) (2014) 1014-1028.

[7] R. Gordon, D. Sinton, K.L. Kavanagh, A.G. Brolo, A new generation of sensors based on extraordinary optical transmission, Accounts of chemical research 41(8) (2008) 1049-1057.

[8] J. Jatschka, A. Dathe, A. Csáki, W. Fritzsche, O. Stranik, Propagating and localized surface plasmon resonance sensing—A critical comparison based on measurements and theory, Sensing and bio-sensing research 7 (2016) 62-70.

[9] T.E. Starr, N.L. Thompson, Total internal reflection with fluorescence correlation spectroscopy: combined surface reaction and solution diffusion, Biophys J 80(3) (2001) 1575-1584.

[10] F. De Lange, A. Cambi, R. Huijbens, B. de Bakker, W. Rensen, M. Garcia-Parajo, N. van Hulst, C.G. Figdor, Cell biology beyond the diffraction limit: near-field scanning optical microscopy, Journal of cell science 114(23) (2001) 4153-4160.

[11] M.J. Levene, J. Korlach, S.W. Turner, M. Foquet, H.G. Craighead, W.W. Webb, Zero-mode waveguides for single-molecule analysis at high concentrations, Science 299(5607) (2003) 682-686.

[12] J. Wenger, Fluorescence spectroscopy enhancement on photonic nanoantennas, Plasmonics in Chemistry and Biology (2019) 139.

[13] H. Ditlbacher, J.R. Krenn, N. Félidj, B. Lamprecht, G. Schider, M. Salerno, A. Leitner, F.R. Aussenegg, Fluorescence imaging of surface plasmon fields, Appl Phys Lett 80(3) (2002) 404-406.

[14] J.-W. Liaw, Analysis of a bowtie nanoantenna for the enhancement of spontaneous emission, IEEE Journal of Selected Topics in Quantum Electronics 14(6) (2008) 1441-1447.

[15] D. Punj, M. Mivelle, S.B. Moparthi, T.S. van Zanten, H. Rigneault, N.F. van Hulst, M.F. Garcia-Parajo, J. Wenger, A plasmonic 'antenna-in-box' platform for enhanced single-molecule analysis at micromolar concentrations, Nat Nanotechnol 8(7) (2013) 512-516.

[16] D.P. Fromm, A. Sundaramurthy, P.J. Schuck, G. Kino, W.E. Moerner, Gap-dependent optical coupling of single "Bowtie" nanoantennas resonant in the visible, Nano Lett 4(5) (2004) 957-961.

[17] A. Kinkhabwala, Z.F. Yu, S.H. Fan, Y. Avlasevich, K. Mullen, W.E. Moerner, Large single-molecule fluorescence enhancements produced by a bowtie nanoantenna, Nat Photonics 3(11) (2009) 654-657.

[18] G.P. Acuna, F.M. Moller, P. Holzmeister, S. Beater, B. Lalkens, P. Tinnefeld, Fluorescence Enhancement at Docking Sites of DNA-Directed Self-Assembled Nanoantennas, Science 338(6106) (2012) 506-510.

[19] E. McLeod, Q. Wei, A. Ozcan, Democratization of nanoscale imaging and sensing tools using photonics, Analytical chemistry 87(13) (2015) 6434-6445.

[20] A. Ozcan, Mobile phones democratize and cultivate next-generation imaging, diagnostics and measurement tools, Lab on a Chip 14(17) (2014) 3187-3194.

[21] S.S.S.C. Sony Corporation, Sony Releases Stacked CMOS Image Sensor for Smartphones with Industry’s Highest*1 48 Effective Megapixels. <https://www.sony.net/SonyInfo/News/Press/201807/18-060E/index.html>, 2018 (accessed 01/30.2019).

[22] U. Security, SONY' S NEW 4K BIG PIXEL SIZE CMOS IMAGE SENSOR IMX380 FOR SMARTPHONE APPLICATIONS. <https://www.unifore.net/product-highlights/sonys-new-4k-big-pixel-size-cmos-image-sensor-imx380-for-smartphone-applications.html>, 2017 (accessed 06/16.2019).

[23] Q. Wei, H. Qi, W. Luo, D. Tseng, S.J. Ki, Z. Wan, Z.n. Göröcs, L.A. Bentolila, T.-T. Wu, R. Sun, Fluorescent imaging of single nanoparticles and viruses on a smart phone, ACS nano 7(10) (2013) 9147-9155.

[24] Q. Wei, W. Luo, S. Chiang, T. Kappel, C. Mejia, D. Tseng, R.Y.L. Chan, E. Yan, H. Qi, F. Shabbir, Imaging and sizing of single DNA molecules on a mobile phone, ACS nano 8(12) (2014) 12725-12733.

[25] Q.S. Wei, G. Acuna, S. Kim, C. Vietz, D. Tseng, J. Chae, D. Shir, W. Luo, P. Tinnefeld, A. Ozcan, Plasmonics Enhanced Smartphone Fluorescence Microscopy, Sci Rep-Uk 7 (2017).

[26] C. Vietz, M.L. Schutte, Q.S. Wei, L. Richter, B. Lalkens, A. Ozcan, P. Tinnefeld, G.P. Acuna, Benchmarking Smartphone Fluorescence-Based Microscopy with DNA Origami Nanobeads: Reducing the Gap toward Single-Molecule Sensitivity, Acs Omega 4(1) (2019) 637-642.

[27] S. Briggs, B. McCall, Count on Your Images: Bringing quantitative imaging to biomedical applications, Optik & Photonik 10(2) (2015) 17-20.

[28] F. Mahdavi, Y. Liu, S. Blair, Modeling fluorescence enhancement from metallic nanocavities, Plasmonics 2(3) (2007) 129-141.

[29] A. Hajiaboli, M. Kahrizi, V.V. Truong, Optical behaviour of thick gold and silver films with periodic circular nanohole arrays, J Phys D Appl Phys 45(48) (2012).

[30] D. Gérard, J. Wenger, N. Bonod, E. Popov, H. Rigneault, F. Mahdavi, S. Blair, J. Dintinger, T.W. Ebbesen, Nanoaperture-enhanced fluorescence: Towards higher detection rates with plasmonic metals, Physical Review B 77(4) (2008) 045413.

[31] L. Wu, P. Bai, X. Zhou, E.P. Li, Reflection and Transmission Modes in Nanohole-Array-Based Plasmonic Sensors, Ieee Photonics J 4(1) (2012) 26-33.

[32] H. Rigneault, J. Capoulade, J. Dintinger, J. Wenger, N. Bonod, E. Popov, T.W. Ebbesen, P.-F. Lenne, Enhancement of single-molecule fluorescence detection in subwavelength apertures, Physical Review Letters 95(11) (2005) 117401.

[33] K.L. Xiong, G. Emilsson, A.B. Dahlin, Biosensing using plasmonic nanohole arrays with small, homogenous and tunable aperture diameters, Analyst 141(12) (2016) 3803-3810.

[34] D. Benke, Improving smartphone cameras with color sensor technology. <https://www.embedded-computing.com/embedded-computing-design/improving-smartphone-cameras-with-color-sensor-technology>, 2016 (accessed 06/16.2019).

[35] IMX214. <https://www.sony-semicon.co.jp/products_en/new_pro/april_2014/imx214_e.html>, 2016 (accessed 06/16.2019).

[36] A.G. Brolo, S.C. Kwok, M.G. Moffitt, R. Gordon, J. Riordon, K.L. Kavanagh, Enhanced fluorescence from arrays of nanoholes in a gold film, J Am Chem Soc 127(42) (2005) 14936-14941.

[37] Y.Y. Chen, A. Kotnala, L. Yu, J.S. Zhang, R. Gordon, Wedge and gap plasmonic resonances in double nanoholes, Opt Express 23(23) (2015) 30227-30236.

[38] B. Schmidt, K. Wetzig, Ion beams in materials processing and analysis, Springer Science & Business Media2012.

[39] C.D. Kinz-Thompson, M. Palma, D.K. Pulukkunat, D. Chenet, J. Hone, S.J. Wind, R.L. Gonzalez, Robustly Passivated, Gold Nanoaperture Arrays for Single-Molecule Fluorescence Microscopy, Acs Nano 7(9) (2013) 8158-8166.